Aero-elastic loads on a 10 MW turbine exposed to extreme events selected from a year-long Large-Eddy Simulation over the North Sea

Gerard Schepers[1], Pim van Dorp[2], Remco Verzijlbergh [2]. Peter Baas[2], Harmen Jonker [2]

TNO Energy Transition, Wind Energy, Petten, 1755LE, The Netherlands
[2]Whiffle, Delft, 2629JD, the Netherlands

Correspondence to: J.G Schepers (Gerard.schepers@tno.nl)

Abstract. In this article the aero-elastic loads on a 10 MW turbine in response to extreme events (low level jet, shear, veer and turbulence intensity) selected from a year-long Large Eddy Simulation on a site at the North Sea are evaluated. These events are generated with a high fidelity LES wind model and fed into an aero-elastic tool using two different aerodynamic models: a BEM based model and a Free Vortex Wake Model. Then the aero-elastic loads are calculated and compared with the loads from the IEC standards. It was found that the loads from all these events remain within those of the IEC design loads. Moreover, the accuracy of BEM based methods for modelling such wind conditions showed a considerable overprediction compared to the Free Vortex Wake model for the events with extreme shear and/or veer.

Notations

BEM	Blade Element Momentum
DEL	Damage Equivalent load
DOWA	Dutch Off-shore Wind Atlas
FVW	Free Vortex Wake
RWT	Reference Wind Turbine
TKE	Turbulent kinetic energy
TI	Turbulent intensity
LLJ	low-level jet

1 Introduction

Given the ambitious targets to decarbonize the global energy system, further progress in wind turbine design remains high at the scientific agenda (Veers et al, 2019). As turbines are becoming larger, they will increasingly operate in atmospheric conditions that are less well captured by traditional wind inflow models that are used in wind turbine design. On the other hand, recent advances in computer science and atmospheric physics have paved the way using high fidelity atmospheric flow models such as Large Eddy Simulation (LES) for wind turbine and wind farm design purposes. This article describes a study

of the simulated loads on a wind turbine in response to extreme wind events modelled with an LES model. It can be considered as a proof-of-concept study to investigate the potential of a coupling between turbine response models and high-fidelity wind models as an alternative to commonly used stochastic wind simulators such as the Swift or Mann model (Winkelaar, 1992, Mann 1998). These simulators model stochastic wind fields in time and space which full-fill pre-defined statistics of e.g. turbulence intensity, coherence etc.

The use of LES to study atmospheric flows through wind farms is gaining popularity in the scientific community. In an overview paper, Mehta et al (2014) discuss several applications of LES in the context of wind turbine loads. One of the strengths of LES that is frequently mentioned by the papers cited in Mehta et al. (2014) is its ability to represent realistic atmospheric conditions in which aspects like shear, veer, stability and turbulence are coherently modeled. The ability of LES to realistically model complex atmospheric flows through wind farms is also stressed by Stevens and Menevau (2017), but, like Mehta et al. (2014), the authors also conclude that LES is computationally too expensive for use in wind farm design. Owing to these computational barriers, the use of LES in an operational context (e.g. for forecasting or for wind resource assessments) or in wind turbine design has so far been limited. Of particular relevance for the present paper, is the work of Storey et al. (2013), who have dynamically coupled an LES model to a detailed turbine model using the FAST aero-elastic code. The two-way coupling realized by Storey et al. (2013) is not pursued in the present paper, where only the turbulent inflow fields are passed on an aero-elastic model. The main novelty that we demonstrate, however, is to move away from the stylized velocity input profiles as input for the LES model. Instead, we use the LES model GRASP (GPU-Resident Atmospheric Simulation Platform) driven by boundary conditions from a global weather model to produce a year-long simulation of the weather at the Offshore Met-Mast IJmuiden. GRASP is computationally optimized and therefore enables detailed modelling of meteorological phenomena on a spatial and temporal grid resolution which is fine enough for aero-elastic load calculations. From the yearly results, we select the five most extreme events in the following categories: shear, veer, turbulence intensity, turbulent kinetic energy and a low-level jet. Special attention will be given to the analysis of results at an extreme low-level jet, since these events are often believed to have significant impact on turbine loading, see e.g. Duncan (2018).

The resulting extreme wind events are then fed as wind input to the aero-elastic solver PHATAS from WMC (now LM) as used by TNO Energy Transition (Lindenburg, 2005) and the aerodynamic modelling from AeroModule tool (Boorsma, K., Grasso, F., & Holierhoek, 2012) which offers the choice between an efficient lower fidelity BEM method and a higher fidely but less efficient Free Vortex Wake Model. The turbine on which the loads are calculated is the 10 MW Reference Wind Turbine as designed in the EU project AVATAR (Sieros, et al., January 2015). The calculated loads as response to these extreme wind events are compared with the loads from a reference design load spectrum which is available from the AVATAR project (Stettner, et al., April 2015). This reference design load spectrum is calculated according to the IEC standards. In this way it can be assessed whether the wind fields from extreme events modeled with LES yield loads that deviate significantly

65 from the design load spectrum. A final topic of investigation is to compare the loads calculated by a model based on blade element momentum theory (BEM) with those from a higher fidelity model: the free vortex wake model AWSM (Boorsma, Grasso, & Holierhoek, 2012). In previous studies indications were found that BEM could overpredict loads for cases with artificial shear (Boorsma, K., Wenz, F., Aman, M., Lindenburg, C., & Kloosterman, 2019). The present study could confirm these findings for realistic shear cases.

70

The work described in the present paper can thus be seen as a proof-of-concept study to explore the merits of using high-fidelity wind simulations as input for load calculations. Such site-specific simulations could someday be done more routinely in wind turbine and wind farm design and could eventually lead to a rethinking of the use of standard design load spectra.

75 The article is structured in the following way: section 2 provides details the wind and turbine modelling details. Section 3 provides the results in two parts: first the wind modelling results are presented and compared with observations. This also serves as a validation of the modelled wind inputs. Secondly, the load results are presented. The comparison between the loads from the extreme events and those from the reference spectrum is given together with an evaluation of results. Conclusions and recommendations for further research are given in section 5.

80 **2 Experimental set-up**

The overall experimental set-up of the research is depicted schematically in Figure 1. Two series of LES runs have been performed: the first one covering the whole year to select the extreme events and the second on to run the selected cases in higher resolution. The wind fields from the selected cases have been passed to the aero-elastic model.
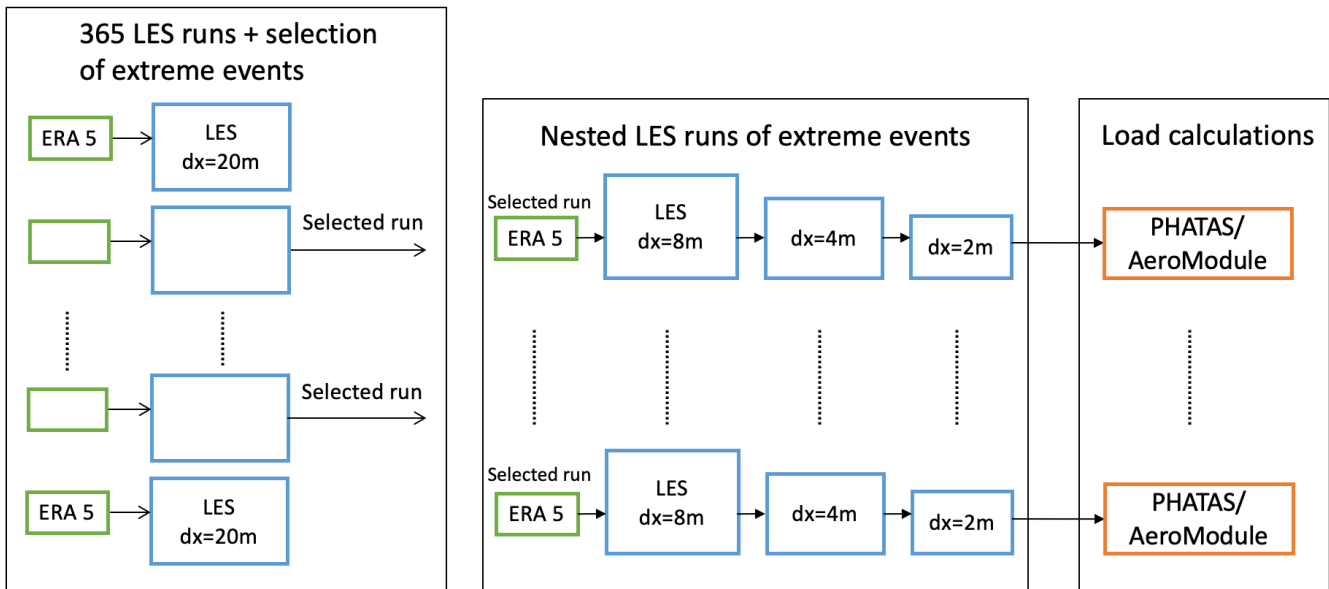
Figure 1 Schematic representation of the experimental set-up. From 365 LES runs for a North Sea location, 5 extreme events are selected. These are re-run on higher resolution and the output passed to the aero-elastic models PHATAS and AeroModule.

2.1 Location

The site for which the LES runs are conducted is the location of the Meteorological Met-mast IJmuiden (MMIJ) in the North Sea, 85 km offshore from the Dutch shore (N52°50.89' E3°26.14'). The mast is shown in Figure 2 and the instrumentation of the mast is given in (Werkhoven & Verhoef, 2012). Measurements are taken with anemometers on a mast which are placed at three different heights above sea level, i.e.: 27m, 58m and at the top level of 92 meter (note that some wind speed sensors are mounted at an altitude of 85 meters as well). They are combined with LIDAR measurements which are taken at 90, 115, 140, 165, 190, 215, 240, 265, 290, 315 meter above sea level.

The observations from the met-mast are not directly used as input for either the LES runs or the load calculations. However, the main benefit of choosing this site for our numerical study is that it allows us to do a validation of the modeled winds against observations.

Figure 2 Meteorological Mast IJmuiden

100

2.2 LES setup

GRASP is a Large Eddy Simulation (LES) model developed by Whiffle that is based on the Dutch Atmospheric Large Eddy Simulation (DALES). The LES code runs on Graphics Processing Units (GPUs) and is therefore referred to as GRASP: GPU-Resident Atmospheric Simulation Platform. GRASP can be run with boundary conditions from a large scale-weather model

105 (Gilbert, et al., 2019) For this study, GRASP has been run for the location of the Meteo Mast IJmuiden in the Dutch North Sea area with boundary conditions from the ERA5 reanalysis dataset (Hersbach et al., 2020) that provides global data of historical atmospheric and ocean conditions. A double periodic LES domain is used to allow full development of the turbulence. As a consequence, the ERA5 boundaries cannot be directly prescribed at the edges of the domain but are prescribed as dynamic tendencies. This means that the rate equations for the LES variables contain an extra term due to large-scale advection. For the

110 velocity components, a second source term accounts for the large-scale pressure gradient as a driving force. More information about this set-up can be found in (Schalkwijk et al., 2015). Driving the LES with boundary conditions from a large-scale weather model, ensures that the full spectrum of atmospheric flow from synoptic to turbulent scales is considered. Amongst others, the interaction between atmospheric stability, turbulence and shear is resolved.

A full year of LES runs of 24 hours each (i.e. 365 simulations of 24 hours, plus a 2-hour spin up period for each simulation)

115 has been performed on a resolution of 20m. From this year of model simulations, several types of extreme wind events have been identified, including low-level jets, high shear, high veer and high turbulence cases. These cases have been re-run and used as boundary conditions for a higher resolution run in the concurrent precursor setting. To this end, a three-way nested simulation has been carried out, see Fig. 3, at 8, 4, and 2 meter resolution with 256 grid boxes in each direction which gives a

domain size of 2x2 km², 1x1 km² and 500x500 m² respectively. The finest grid with a resolution of 2 meter yields 51 wind

120 speed points over the 103 meter AVATAR blade radius. The finest temporary resolution is 10 Hz which yields an azimuth interval of 6 degrees at the rated rotor speed of 10 rpm (which is in the order of intervals used in aero-elastic simulations). The computation time of the year of LES runs on 20m resolution amounts to roughly 2 days on a cluster with 4 NVIDIA Volta GPUs plus some additional runtime for the selected high-resolution runs. The chaotic character of the wind field in Figure 3 illustrates the realistic representation of atmospheric turbulence in the model as well as the nesting settings.

125
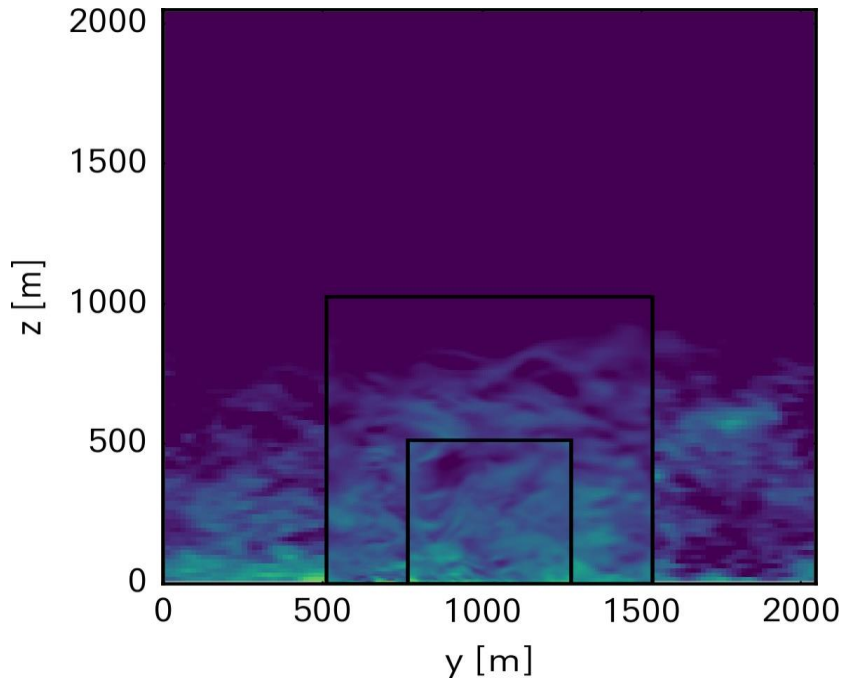
Figure 3 Vertical cross-sections of wind speed in the three different nested LES runs. The coarsest runs use periodic lateral boundary conditions and large-scale forcing from ERA5. The higher resolution runs use lateral boundary conditions from the 'upper' nests

2.3 Reference turbine

130 The turbine that is used for the load calculations is the AVATAR Reference Wind Turbine (RWT) (Sieros, et al., January 2015). This is a turbine with a rated power of 10 MW as designed in the EU project AVATAR. The AVATAR RWT is a low induction variant of a 10 MW RWT designed from the EU Innwind.EU project, see Bak, et al. (2013). The main characteristics of the AVATAR RWT listed in table 1.

The low induction concept used in the AVATAR RWT makes an increase in rotor diameter possible from D = 178 meter (i.e.

135 the diameter of the Innwind.EU RWT) to D= 205.8 meter with a limited increase in loads. The hub height of the AVATAR RWT is 132.7 meter by which the lowest point of the rotor plane is at an altitude of 29,8 meter and the upper part of the rotor

plane is at 235,6 meter. The rated rotor speed is 9.8 rpm. All design data (the aerodynamic and aero-elastic data of blades, tower, shaft and other components) of the AVATAR RWT are publicly available (Sieros, et al., 2015).

140   A controller has been designed that covers two regimes. Below rated wind speed, the controller aims for maximum power production with variable rotor speed operation using a speed dependent generator torque setpoint (for optimum tip speed ratio) and constant optimal blade pitch angle. Above rated wind speed, the rotor speed and generator power are regulated to their nominal rating using constant generator torque and collective blade pitch control.

145   As a reference case to compare the loads resulting from the extreme events from the LES with, a standard design load spectrum has been calculated (Stettner, et al., 2015). The calculations of the design load spectrum have been repeated with the most recent versions of design tools to assure consistency in tools.

Diameter	205.8 m
Hub height	132.7 m
Altitude of lowest and upper point of rotor plane	29.8 m-235.6 m
Rated rotor speed	9.8 rpm
Mean axial induction factor	0.24

Table 1: Main characteristics of AVATAR RWT

150

2.4 Aero-elastic modelling of extreme events

The aero-elastic loads in response to the extreme GRASP cases are calculated with the PHATAS code (Lindenburg, 2005) using two different solvers: one based on Blade Element Momentum (BEM) theory and one based on the free vortex wake model. The development of the PHATAS code started in 1985 by ECN (now TNO) but later the code has been transferred to

155   WMC (now LM). The code takes into account blade flexibilities in all three directions (flatwise, edgewise and torsional) but also tower and drive train flexibilities. Furthermore the control of the AVATAR turbine as described in section 2.3 is taken into account.

The default aerodynamic solver of PHATAS is based on Blade Element Momentum (BEM) theory. This is an efficient but lower fidelity model which, because of its efficiency is used for industrial design calculations. In its basis a BEM model is

160   steady and 2D, by which phenomena like yaw and stall are calculated with a very large uncertainty. Therefore, in the last decades several engineering models have been developed which are added to the BEM theory. These engineering add-ons cover phenomena like unsteady and 3D effects as well as yaw and stall. They are still of a simplified efficient nature which

makes them suitable for industrial calculations. These engineering models are validated and improved with the most advanced measurement data (Schepers J. G., November 2012) and with high fidelity models (Schepers J.G. et al, 2018)

165   The GRASP events are calculated with a PHATAS version which is linked to an alternative aerodynamic solver AeroModule as developed by TNO. AeroModule is a code which has an easy switch between an efficient BEM based model and a high fidelity but time-consuming free vortex wake based model AWSM (Boorsma, Grasso, & Holierhoek, 2012). This allows for a straightforward comparison of these two models with precisely the same input. In this way it can be assessed how well the load response is calculated with a BEM model in comparison to the load response as calculated from the higher

170   fidelity model AWSM.

In the present study the blade root flatwise moment is considered. Both extreme loads and the Damage Equivalent fatigue Loads (DEL) are considered where the latter is based on a Wohler slope of 10. It is noted that the Damage Equivalent Load translates the underlying rain flow cycle spectrum into a single number. This facilitates the presentation of results, but it conceals the underlying frequency information from the rain flow cycle spectrum. The loads are calculated in the coordinate

175   system from Germanischer Lloyd.

The computation time of the load calculations is much faster than real-time for BEM on a simple laptop. The Free vortex wake calculations are a factor 100-1000 slower (dependent on number of wake points and the wake cut-off length etc).

2.5 Interface between GRASP and PHATAS

180   The input for AeroModule (and so PHATAS) consists amongst others of the 3D wind speeds at several locations in the rotor plane as function of time. For the present study they were supplied by Whiffle in separate files in NETCDF format in the resolution which is given in section 4.1.1. They were transformed by ECN part of TNO into TurbSim wind simulator files (Jonkman, 2009). The turbine yaw angle is fixed and aligned with the time averaged wind direction at hub height from the GRASP wind input.

2.6 Calculation of reference design load spectrum

185

The reference design load spectrum for the AVATAR RWT has been calculated and assessed in Stettner, et al., (2015). It is calculated along the IEC standards for wind class IA, which was considered representative for offshore conditions by the AVATAR consortium. As mentioned before this is a conservative turbulence class for the present location.

The load spectrum from (Stettner, et al., April 2015) covers normal production (DLC 1.2), standstill, stops etc. In the present

190   study it is only the normal production cases from DLC 1.2 which are repeated. In section 6. it will be shown that these cases are sufficient for the present assessment and there is no need to include special cases.

The reference load cases are carried out as 10-minute time series for mean wind speeds ranging from 5-25 m/s, with a wind speed interval of 2 m/s, a shear exponent of 0.2, where the wind input is generated from the stochastic wind simulator SWIFT using 6 different seeds. A small yaw angle of 8 degrees is included to account for yaw control tracking errors.

195

It is noted that the aerodynamic model with which the reference spectrum is calculated is based on the default BEM model of PHATAS where the GRASP events from section 4 are calculated with both BEM and FVW. Apart from fundamental model differences between BEM and FVW all calculations are carried out in exactly the same way, with the same degrees of freedom, engineering models used etc., in order to assure consistency in results.

200 3 Results

3.1 LES wind output

The GRASP simulations were carried out from 2014/12/1 to 2015/12/1. Fig. 2 presents a comparison between modeled and observed 92-m wind speed for the entire year in the form of a scatter density plot. The agreement between the modeled and observed 92-m wind speeds is good and no clear bias is observed. A more elaborate comparison of the yearly LES results against the MMIJ observations could provide additional insights in the performance of the LES model for specific atmospheric

205 conditions, but this is not pursued in this paper. A more in-depth comparison of LES winds against North Sea observations is presented in Wiegant & Verzijlbergh (2019). However, in section 3.2 the yearly LES results are analysed in the light of their correspondence with observed turbulence, extreme shear, extreme veer and low-level jets.
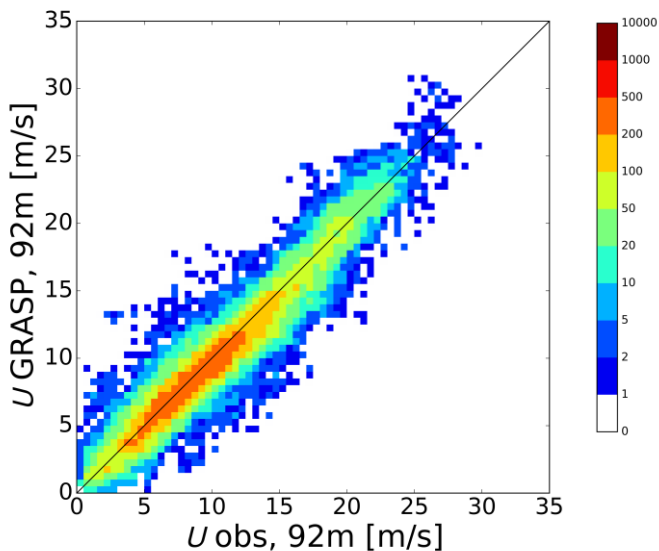
210 **Figure 4 Scatter-density plot of modeled versus observed 92-m wind speed.**

From the yearly LES data, the following five "extreme" cases of 10 minutes were selected:

- Strongest low-level jet (LLJ). The LLJ's were detected with the algorithm from Baas (2009).
- Strongest wind veer over the rotor.
215 - Strongest shear over the rotor.
- Highest turbulence kinetic energy (TKE) below cut-out wind speed.
- Highest turbulence intensity (TI) around rated wind speed (i.e. higher than 10 m/s) and lower than cut-out

For each of these five selected cases, a 3-fold nested simulation was performed with a spatial resolution of 2 meters and a
220 temporary resolution of 0.1 seconds for the finest nest. Figure 5 presents an overview of the selected extreme wind cases. For
each extreme wind case (columns), profiles of wind speed (U), wind direction (phi), turbulence intensity (TI) and turbulent
kinetic energy (TKE) are shown (rows). For comparison, also the MMIJ observations and ERA5 reanalysis data are added.
Although ERA5 profiles have not been used further in the analysis, showing their profiles together with the LES profiles gives
an indication of how different representation of turbulent transport in the LES model leads to different vertical wind speed
225 profiles. Although the significance of a one-to-one comparison of modeled and observed 10-minute records is limited,
especially when considering extreme events, clear correspondence between the model results and the observations is observed.
In Section 4.1.3 the modeled extreme events are discussed from a climatological point of view.

For the strongest low-level jet, Fig. 4 shows that the wind speed at the lowest point of the rotor plane is approximately 9.2 m/s,
230 then increases to a maximum value of almost 13 m/s. This value is reached slightly below hub height. Above hub height the
wind speed decreases to approximately 10.3 m/s at the upper part of the rotor plane. The wind speed variation with height goes
together with a relatively large veer from approximately 230 degrees at the lowest point of the rotor plane to 239 degrees
slightly below hub height above which it remains more or less constant. It must be noted that a shear exponent of 0.2 (i.e. the
exponent used in the IEC reference load spectrum, see section 5) at a comparable hub height wind speed of 13 m/s yields a
235 velocity of 9.7 m/s at the lower part of the rotor plane. In other words, the shear prescribed by the standards is only slightly
less than the shear from the LLJ in the lower part of the rotor plane. For the selected LLJ case the corresponding observed
wind profile does not show a jet-like profile. In Section 4.1.3 it will be shown that on a climatological basis modeled and
observed low-level jets have similar characteristics.

The strongest wind veer case shows a wind direction of approximately 85 degrees at the lowest part of the rotor plane and a
240 wind direction of approximately 120 degrees at the upper part, leading to a wind direction difference of 35 degrees. The
correspondence with observations is reasonable. Note that for this strong veer case but the observed and modeled wind speed
profiles show a clear LLJ.

The strongest shear case shows a wind speed of approximately 11.5 m/s at the lowest part of the rotor plane above which it
increases to almost 16 m/s at hub height above which it increases further to approximately 19 m/s at the upper position of the

245 rotor plane. The observations show a comparable wind shear. We selected the largest wind speed difference over the rotor plane, which turned out to be 8.5 m/s. Again, it must be noted that a wind shear exponent of 0.2 (i.e. the exponent prescribed in the standards for the normal operating condition cases) and a hub height wind speed of 16 m/s already gives a wind speed difference of 6.2 m/s over the rotor plane.

For the case with extreme turbulence intensity and extreme turbulent kinetic energy, the turbulence intensities at hub height

250 are found to be approximately 5% and 6.5% at approximately 14.8 m/s and 22.5 m/s respectively. Although these turbulence intensities are the highest for the selected year, they are much lower than the values for turbulence class A at the corresponding wind speeds (approximately 18% and 16%). This indicates that the reference design load spectrum as calculated in the AVATAR project is conservative for isolated turbines at the selected site. However even a turbulence class C (the lowest possible turbulence class in IEC) leads to turbulence intensities which are still far above the extreme

255 turbulence intensities in the selected year.

It is also important to note that the extreme shear and extreme low-level jet cases go together with very low turbulence levels. This is shown in table 1, which gives the turbulence intensity as function of height for the LLJ event.

Height [m]	Turbulence intensity [%]
31	5.8
81	3.3
133	1.6
185	1.3
235	1.2

260 Table 2: Turbulence intensity as function of height for the extreme low-level jet case

The turbulence intensity at hub height is 1.6%. This low turbulence intensity should be kept in mind when analyzing the load results. The turbulence intensity decreases from 1.6% at hub height to 1.2% at h = 235 meter despite the decreasing wind speed above hub height in Fig. 2. This implies that the decreasing turbulence intensity with height should be attributed to a

265 strong decrease in standard deviation of wind speed fluctuations which overcompensates the decreasing wind speed. In fact, this is what can be expected under the strongly stratified conditions that favor the formation of LLJs. In contrast, for the LLJ case the observed values of TI do increase with height, which would be much harder to explain. Note that estimating turbulence quantities from LiDAR observations is not trivial, see e.g. Sathe at al. (2011).
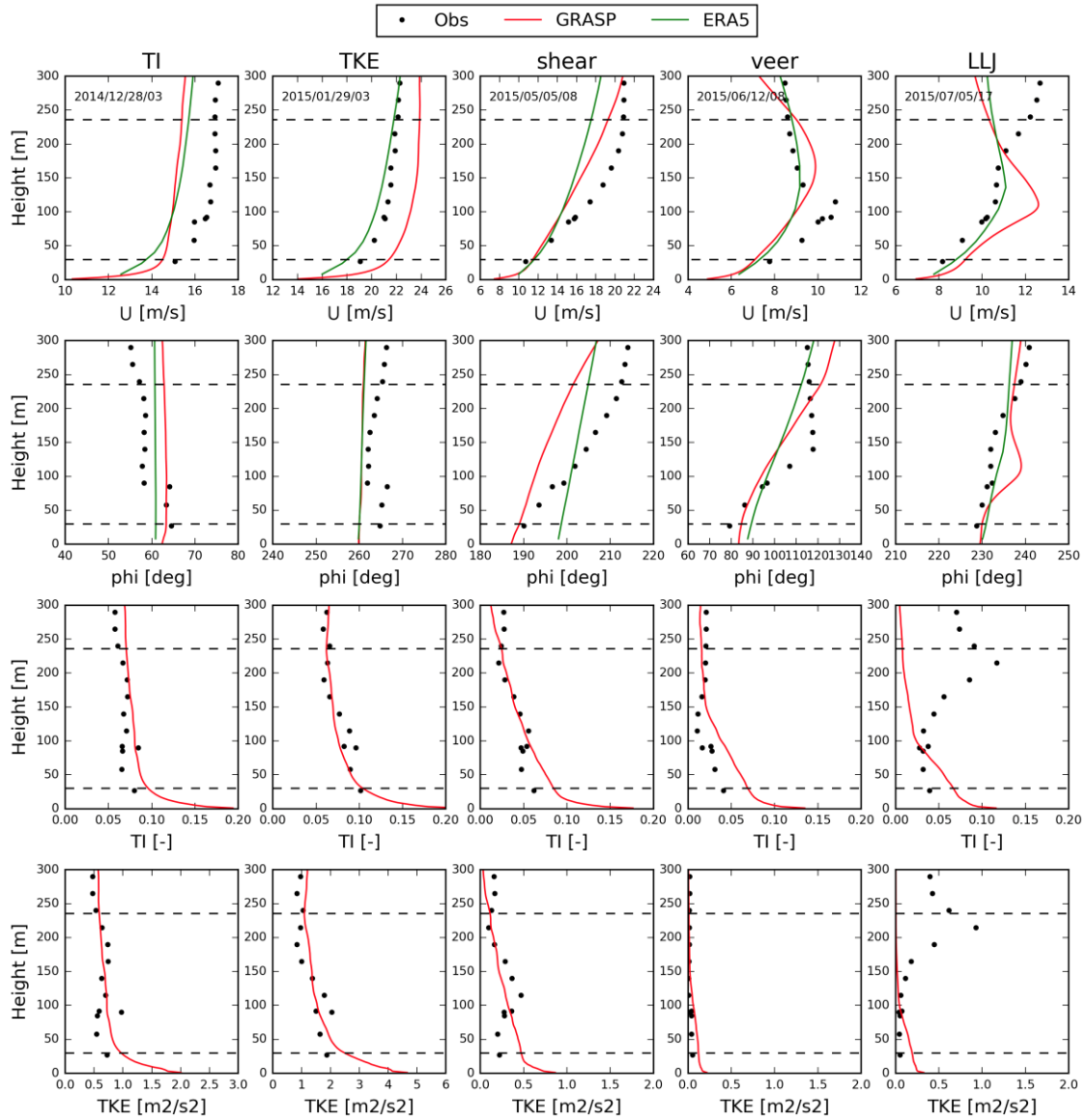
270

Figure 5 Profiles of four meteorological quantities (wind speed U, wind direction phi, turbulence intensity TI and turbulent kinetic energy TKE) for the five selected extreme cases (different columns) with high TI, TKE, wind shear, veering, and a strong LLJ. Observations are indicated as black dots, the high-resolution GRASP (2m grid-spacing) results in red, and ERA5 reanalysis data in green. Dashed lines indicate the upper and lower part of the rotor plain.

275

3.2 Climatology of extreme events

Instead of a one-to-one comparison of isolated 10-minute records, here we compare the climatology of extreme wind events from the yearly GRASP LES results and the observations. Figure 6 shows profiles of wind speed and veering with height for the 90th percentile of strongest shear and veer conditions between 215 and 90 m. For strong shear conditions (left) the GRASP
280   and ERA5 wind speed profiles are close to the observations. For these cases the wind direction changes only weakly with height and is slightly larger in the observations than in the model. For strong veer conditions (right) the wind speed is weak and constant with height above roughly 90 m. The strong veering of the wind with height is well-represented by GRASP and underestimated by ERA5. This is clearly an example where the different representation of turbulent mixing in an LES model compared to a numerical weather prediction (NWP) model leads to a different wind speed profile.

285
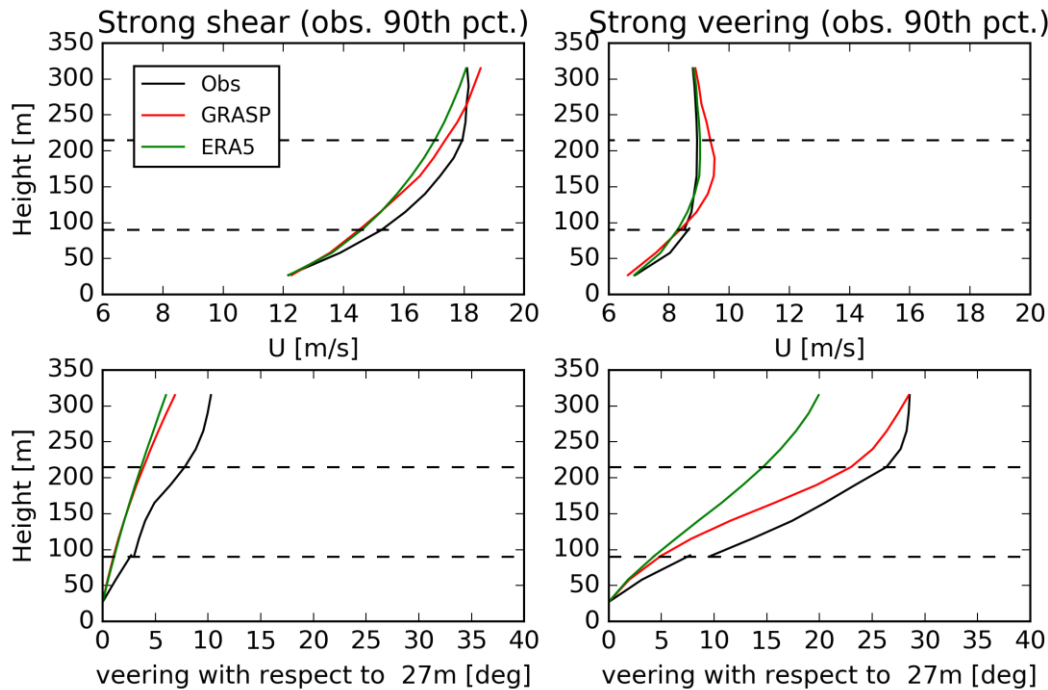
Figure 6 Comparison of the 90th percentile strongest shear (left) and veer (right) conditions from observations, ERA5 and GRASP.

In Figure 7 the standard deviation of the wind is plotted versus the wind speed for the 92-m level. The top panels include one year of observations and simulations. The division of these two quantities gives the TI. For reference, lines of equal TI of 5% and 10% are indicated. Clearly, stronger winds yield more intense fluctuations. The model tends to have slightly higher TI
290   values than observed, but the difference is within a few percent. For wind speeds of around 10 m/s, the observed and modeled TI values are mostly close to 5%.

In section 6 of this paper, it will be shown that the loads from the LLJ are relatively low. The low loads at LLJ are partly caused by the very low turbulence intensities which go together with an LLJ. This raises the question whether these low

turbulence intensities at LLJs are also found in the measurements. Therefore, the lower panels of Figure 7 only include data
points that satisfy the criterion for the occurrence of a low-level jet. Both in the observations and the LES results, the TI
values of LLJ events are generally in the range of 2% (sometimes even less than 1%) at an altitude of 92 meter. This can be
seen as a confirmation that such low turbulence intensities are found at LLJ events and are well represented by the LES
model.
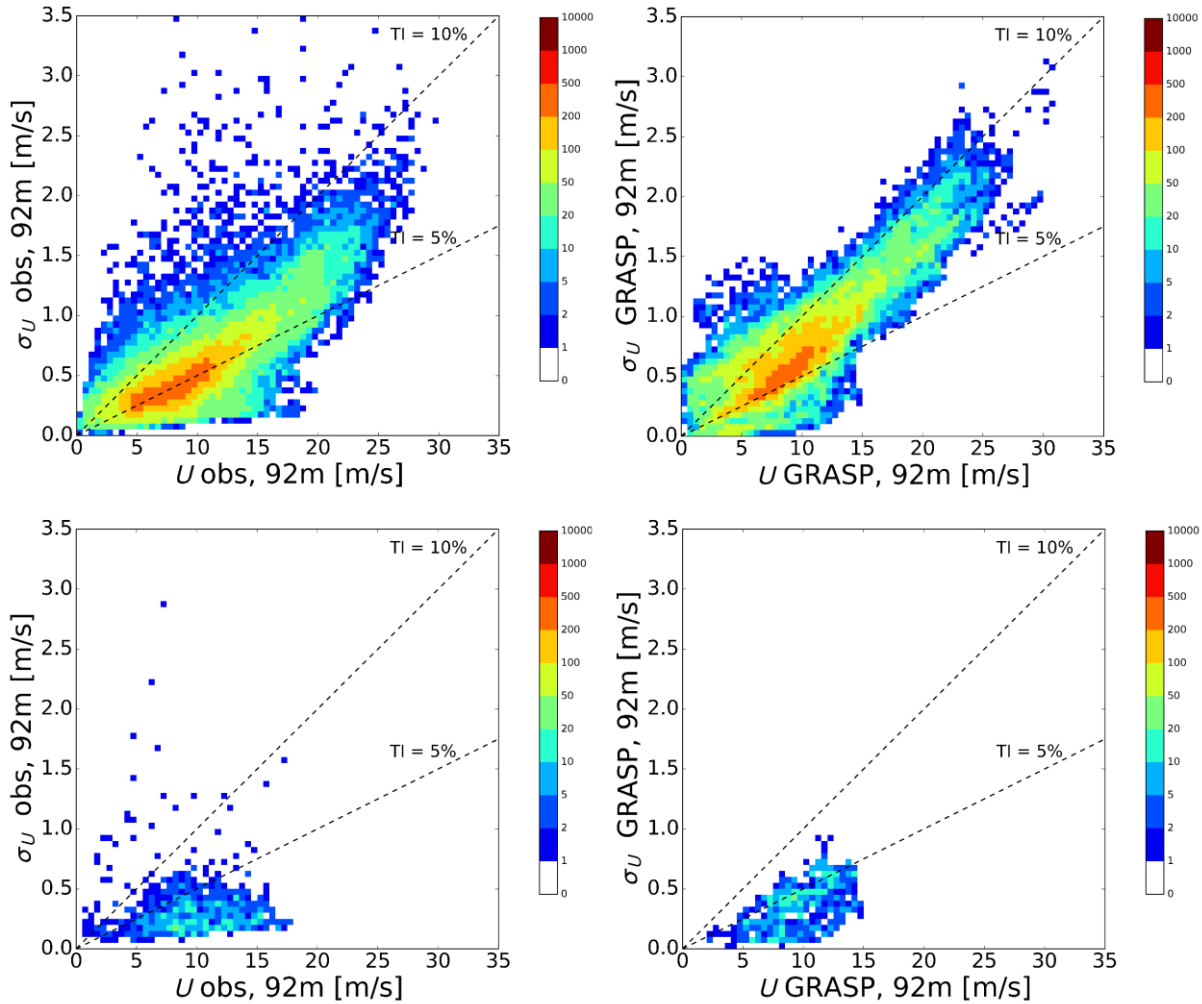
Figure 7 Scatter-density plot of the standard deviation of the wind speed versus the wind speed at the 92-m level. Left panels: observations; right panels: model results, Top panels: entire year; lower panels: only LLJ cases.

Figure 8 shows average low-level jet wind speed profiles for the observations, GRASP and ERA5, i.e. the profiles averaged
over all timestamps of the respective dataset when a LLJ was present according to the LLJ criterion (Baas et al, 2009). The
agreement between GRASP and the observations is within roughly 0.5m/s, whereas ERA5 underestimates the speed of the

LLJ by approximately 2 m/s. The frequency of LLJ occurrence is highest in the observations with 4.8 % of the 10-minute records. For GRASP and ERA5 the LLJ frequency amounts to 2.3% and 0.6%, respectively.
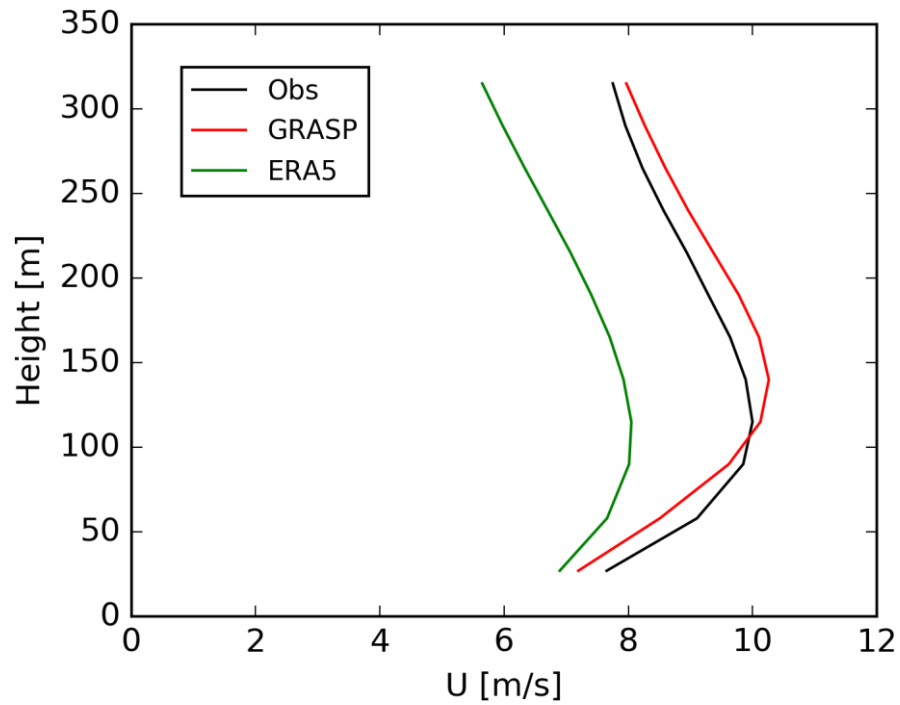
Figure 8 Average low-level jet wind speed profiles.

3.2.1 Concluding remarks on wind validation

In summary, the extreme wind cases that were selected based on GRASP model output, represent 'real weather'. That is to say, there is a strong qualitative and often quantitative agreement between the modelled and observed extreme events of LLJ, wind shear, veer, TI and TKE. Although the agreement for the selected LLJ is moderate, it is encouraging to see that many other LLJ events in the year of simulation find a shear which is comparable to the measurements. Moreover, most LLJ's go together with low turbulence levels and large veer in both calculations and measurements. In general, the climatology of the extreme events (shear, veer, TI, TKI and LLJ) as modeled by GRASP resembles the observed extreme events well.

3.3. Comparison between aero-elastic loads at extreme events with loads from the reference spectrum

Figure 9 shows the resulting equivalent fatigue flatwise moment as function of the 10-minute averaged wind speed from the reference design load spectrum and extreme GRASP events. The values indicated with *reference* are the loads as calculated for DLC1.2. They are compared with the BEM and AWSM calculated loads for the case of extreme low-level jet (*LLJ*), Veer, Shear, Turbulence Intensity (*TI*) and Turbulence kinetic energy (*TKE*).
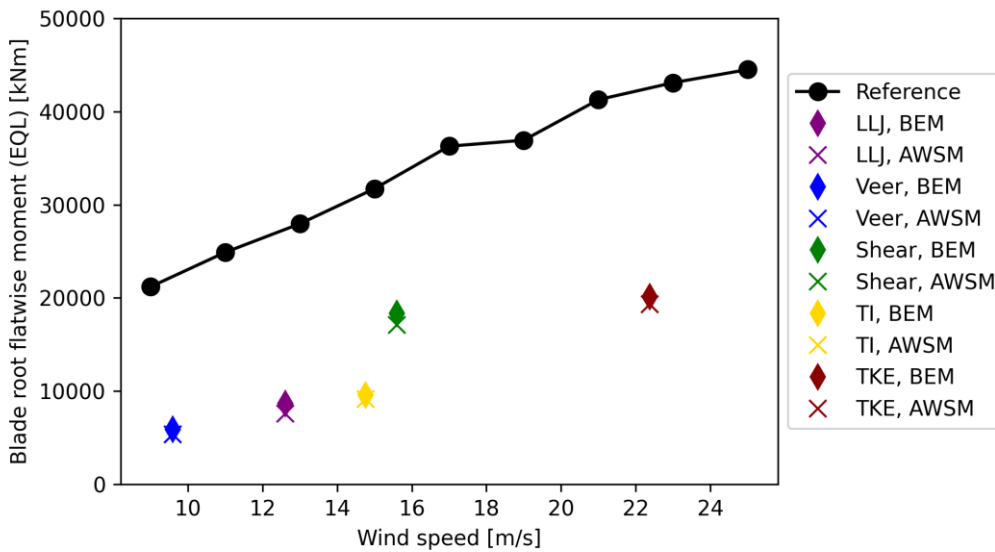
Figure 9 Equivalent blade root flatwise moment: DLC1.2 versus GRASP extreme wind events
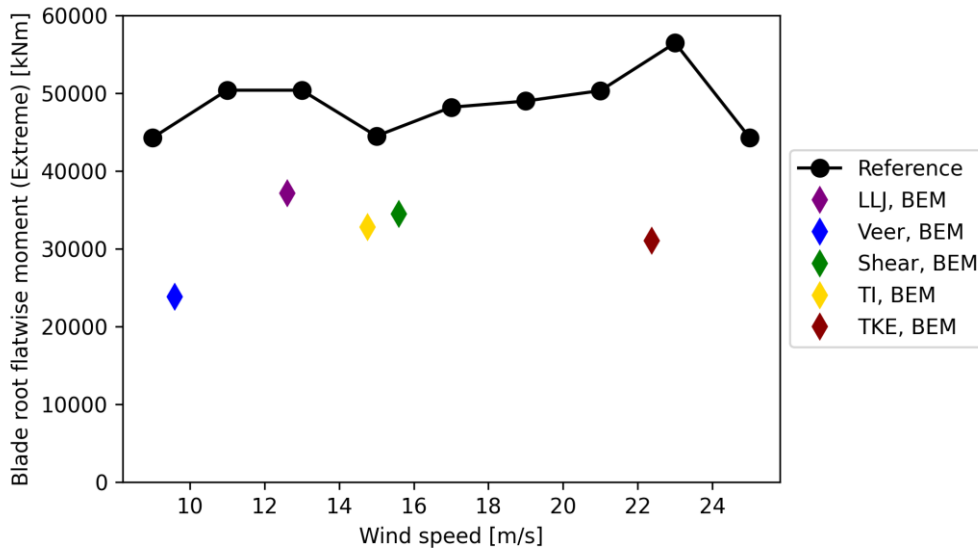
 Figure 10 Extreme blade root flatwise moment: DLC1.2 versus GRASP extreme wind events.

In Figure 10, the extreme flatwise moment as extracted from the 10-minute time series is compared and again plotted as function of wind speed. The extreme load has been extracted for a BEM based calculation only. The presentation of extreme loads as function of wind speed may not be the most relevant metric for design purposes, since it is the overall maximum value

330   which determines the design. This way of presenting is chosen because it shows the wind speeds where the extreme events are found. In all cases the extremes were found to be the maximum positive values (using the sign conventions from the GL coordinate system). The design load spectrum has been calculated for 6 different seeds per wind speed. The results from Figure 9 is based on the averaged equivalent load. The values from Figure 10 are the overall extremes per wind speed.

The present analysis is based on normal production cases (DLC 1.2) only which means that special and extreme load cases are

335   excluded. As such the actual maximum extreme load from a full IEC spectrum could even be higher than the values presented in Figure 10. Some indication for that is found in (Savenije, et al., December 2017) which shows that often non DLC 1.2 cases (e.g. DLC 6.2, idling at storm loads) are more extreme indeed.

In order to gain some further understanding on the results, the loads from the low-level jet are analyzed in more detail. Table 3 compares the DEL of the flatwise moment from DLC1.2 at 13 m/s (second row) with those from the Low Level Jet as

340   calculated with BEM (third row) and AWSM (fourth row). Note that the wind speed of 13 m/s is very close to the 10-minute averaged hub height wind speed at the low-level jet. In the second column the DEL of the full load is calculated, which corresponds to the results from Figure 9.

The third column gives the DEL from the azimuthally binned averaged variation. This azimuthally binned averaged variation is (for a linear system) similar to the deterministic variation which is mainly a result of the shear (although the veer in the

345 LLJ event and the 8 degrees yaw error for DLC 1.2 leads to a deterministic variation as well). The equivalent loads from the
deterministic variation are calculated for the BEM results only. All DEL's are normalized with those from the full load of
DLC1.2

	$M_{flat, DEL}$ [Nm]	$M_{flat, DEL}$ deterministic [Nm]
DLC1.2(BEM), 13 m/s	1.000	0.568
LLJ(BEM)	0.310	0.307
LLJ(AWSM)	0.272	

350 Table 3: Comparison of equivalent blade root flatwise moment for extreme low-level jet (relative to the DEL of DLC 1.2)

3.3.1 Assessment of loads from extreme events

An important observation is that the loads in response to the extreme wind events from GRASP remain within the load envelope
of the reference spectrum. This is true for the equivalent fatigue loads (see Figure 9), which shows that all DEL's from the
355 GRASP extreme events are lower than the DEL's from the reference DLC 1.2 at comparable wind speeds. It is also true for
the extreme loads, see Figure 10. As explained above the "real" extreme reference loads are likely to be even higher than the
values given in these figures, since the results in these figures consider DLC 1.2 only. This makes that the extreme loads from
the GRASP wind events remain within the reference spectrum within an ever wider margin.

From table 2 it can be concluded that the equivalent flatwise moment at the LLJ is only 31% (approximately) of the equivalent
360 load from DLC 1.2. The modeled wind profiles and turbulence levels during the LLJ events provide some further insights on
this. As mentioned in section 4.1.2 the turbulence level at the low-level jet is extremely low (approximately 1.6 % at hub
height) where the turbulence level for DLC1.2 at 13 m/s is in the order of 19%. The very low turbulence level at the LLJ
explains, at least partly, the much lower fatigue load. This is confirmed by the DEL of the deterministic variation in the third
column which is almost similar (99%) to the DEL of the total variation in the first column. The 1% difference is the addition
365 from turbulence and should be compared with the difference between deterministic and total variation from DLC 1.2 which is
approximately 43%. This indicates how little the low turbulence level at the LLJ adds to the fatigue loads.

Still the DEL of the deterministic variation at the LLJ is much lower (approximately 54%) than the DEL of the deterministic
variation at DLC 1.2. This indicates that the low fatigue loads at a LLJ are not only caused by the lower turbulence level, but
it is also the different shear from the LLJ which lowers the DEL. Some further explanation is offered by Figure 11, which
370 shows a comparison between the azimuthally binned averaged flatwise moments for the LLJ and DLC1.2. Azimuth angle zero
indicates the 12 o'clock position. The rotor rotates clockwise so azimuth angle 90 indicates the 3 o'clock position when looking
to the rotor. The variation from DLC 1.2 has a 1P variation with a relatively large amplitude. This is the behavior of the flatwise

moment in an atmosphere with 'common' vertical wind shear. The wind speed (and so the loads) decreases when the blade rotates from the vertical upward 12 o'clock (zero azimuth) position to the vertical downward 6 o'clock (180 azimuth). The

375   flatwise moment increases again when the blade rotates from 180 degrees towards 360 degrees.

The azimuthal variation in flatwise moment from the low-level jet is very different from the variation which results from DLC1.2. It shows a 2P variation with a relatively small amplitude. This 2P variation can be explained with the LLJ wind speed profile from Figure 5 which shows the wind speed to be low at 0 degrees azimuth (the 12 o'clock position, when the blade is pointing vertical upward) and at 180 degrees (the 6 o'clock position, when the blade is pointing vertical downward). The wind

380   speed is maximum at (approximately) hub height which correspond to azimuth angles of 90 and 270 degrees (i.e. the 3 o'clock and 9 o'clock position when the blade is standing horizontally). This velocity variation is reflected in the flatwise moment. It is low at 0 degrees, high at (roughly) 90 degrees and 270 degrees and low again at 180 degrees. This leads to a 2P variation, but the load amplitude is relatively small. Hence, although the 2P load variation happens twice as often as the 1P load variation from   the   DLC   1.2.   the   lower   amplitude   of   the   variations   leads   to   a   lower   fatigue.

385   It is noted from Figure 5 that the present LLJ has a maximum velocity close to hub height and it could be argued that a different hub height leads to a different load behavior. The lowest part of the rotor plane of the AVATAR RWT is at an altitude of 29.8 meter and the upper part is at an altitude of 235.6 meter. It was not considered feasible to decrease the tower height and lower the rotor plane even more. Also, a lowering of hub height would bring the maximum in LLJ wind speed even closer to hub height (See Fig. 4). Therefore, an increase of tower height has been investigated but this was limited by the domain size of

390   the GRASP field which extends up to a maximum altitude of 255 meter. Hence the tower height cannot increase with more than 19.4 meter. A hub height of 250.7 meter has been investigated but this did not lead to significantly different conclusions (i.e. the loads from the LLJ remain within those of the reference spectrum). Alternatively, a LLJ event that has its wind maximum at a different height (e.g. at the top of the rotor plane) could lead to a markedly different load behaviour.

395   **3.3.2 Accuracy of calculating loads from extreme events**

From Figure 9 and table 3 it can be concluded that the DEL of the blade root flatwise moment is overpredicted with the BEM model (assuming that the fatigue loads as calculated with the FVW model AWSM are close to reality). Similar observations were made in (Boorsma, Chasapogianis, Manolas, Stettner, & Reijerkerk, September 2016) and (Boorsma, Wenz, Aman, Lindenburg, & Kloosterman, September 2019) where differences are reported in the order of 10-20% for load

400   cases which are representative to IEC normal production. The present study shows overpredictions which are in the same order of magnitude i.e. 14% for the extreme LLJ, 11% for the extreme veer case, 7% for the extreme shear case but only 4-5% for the extreme turbulence intensity and turbulent kinetic energy. The difference between AWSM and BEM based fatigue shaft loads (not shown in this paper) were generally found to be smaller and less straightforward than for the blade root flatwise moment: in some cases, AWSM even predicts higher fatigue loads than BEM.

405   The commonly believed explanation for the overpredicted BEM DEL lies in a more local tracking of the induced velocity variations in FVW models, by which they vary synchronously with the variation in inflow. This synchronization then damps

out the variations in angle of attack. It should then be noted that the AVATAR RWT is a low induction concept, i.e. a concept which is less sensitive to such induction driven phenomena. This makes it plausible that the difference for conventional turbines with higher induction are even larger. Moreover, FVW models allow for a more intrinsic and realistic
410 modelling of shed vorticity variations in time.
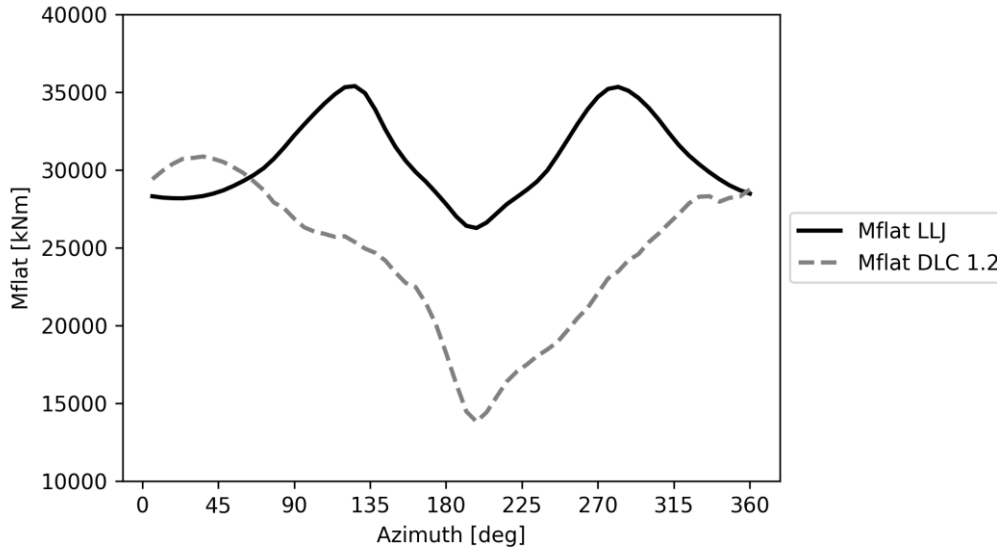
Figure 11 Azimuthally binned averaged flatwise moment: LLJ versus DLC1.2

4 Conclusions and recommendations

415 This paper has described a study in which turbulent wind fields generated with LES were passed to the aero-elastic code PHATAS (with AeroModule) from ECN part of TNO. The wind fields corresponded to extreme events selected from a 1-year simulation of the LES wind fields. These events are fed as wind input files to the PHATAS code and used to simulate the AVATAR 10 MW Reference Wind Turbine (RWT) at an offshore location.

A validation of the LES wind fields has taken place by comparing the calculations with measurements from Meteorological
420 Mast IJmuiden. This validation shows that there is generally a good agreement in the load determining characteristics of the LES wind fields by which the calculated events can be used with confidence to assess the importance of them in an aero-elastic load context. However, more validation is needed, in particular on turbulence characteristics at high altitudes (say higher than 100 meter)

The resulting (DEL and extreme) loads for the selected events are (roughly speaking) 30-70% lower than those from the
425 reference design load spectrum of the AVATAR RWT. As such, the often-heard expectation that low-level jets have significant impact on loads is not confirmed for the present offshore situation. This is partly explained by the low turbulence intensities

(roughly 1-2%) which go together with the LLJ. However, the deterministic DEL from the LLJ shear is also lower than the deterministic DEL from DLC 1.2. This is due to the fact that the shear from the LLJ is not extreme in comparison to the shear from the IEC standards. The LLJ shear profile then leads to a 2P variation instead of a 1P variation from 'normal shear' but
430 the amplitude is smaller resulting in a lower fatigue damage. From the results one could hypothesize that the combination of the shear and turbulence levels from the IEC standards may often lead to conservative loads. However, more research is needed to warrant a conclusion, especially in the validation of the on-site turbulent wind fields.

It is noted that the present LLJ has, more or less by coincidence, a maximum velocity close to hub height. A study on different hub heights didn't show a very different outcome but the limited domain size of the LES wind field made that the hub height
435 could not increase with more than 20 meters. A study with a much taller tower (and so an extended domain size) is recommended.

For the selected extreme events the DEL from the more physical AWSM model are considerably lower than the DEL of BEM model which indicates that BEM overpredicts fatigue loads. The difference is largest for the shear driven cases and for a rigid construction. Efforts should be undertaken to improve the BEM fatigue calculations for such shear events.
440 The present research can be considered as a proof-of-concept study to investigate the potential coupling between turbine response models and high-fidelity wind models. The demonstrated computational feasibility and the results lead to the recommendation to explore such coupling even further for the calculation of a full design load spectrum. This makes it possible to assess the validity of a conventional method for the calculation of a design load spectrum based on stochastic wind simulators. The higher fidelity of the present method makes that eventually design calculations could be based on physical
445 wind models. Future work should focus on applying and validating this method in more challenging case studies, such as in full-scale wind farms where the down-stream turbulence is heavily affected by the turbines themselves. Including other wind turbines in the LES domain also has the benefit that the implicit assumption that the upstream turbulence is not affected by the turbine can be overcome. Finally, we recommend to also study situations where turbines are situated in complex terrain environments.
450 Although the coupling between PHATAS and GRASP was proven feasible, the interfacing through GRASP output and PHATAS wind input files can be improved. Ideally an on-line coupling should be developed without the need of interface files. This would also enable a two-way coupling, where force components and blade positions are passed back to the LES model during run-time.

455 **Author contributions and acknowledgement**

Author contributions. J.G. Schepers assembled and ran the load simulation results and analyzed the overall results. P. van Dorp and H.J.J. Jonker modified the LES code and performed the GRASP simulations. R.A. Verzijlbergh assisted in the analysis of the results. P. Baas performed the validation of the GRASP simulations

Acknowledgement The research was carried out within the Dutch national project DOWA in sponsored by the Topsector
460   Energy Subsidy from the Ministry of Economic Affairs and Climate; F. Savenije (ECN part of TNO) is acknowledged for the
calculation of the reference load spectrum. K. Boorsma (ECN part of TNO) is acknowledged for his support on the AeroModule
code.

Competing interests. The authors declare that they have no conflict of interest.

465

Bibliography

Baas, P. B. A climatology of nocturnal low-level jets at Cabauw. *Journal of Applied Meteorology and Climatology, 48(8),*,
1627-1642, 2009

Bak, C., Zahle, R., Bitsche, R., Kim, T., Yde, A., Henriksen, L., . . . Natarjan, A. *The DTU 10 MW Reference Wind Turbine.*
470   Danish Technical University, 2013.

Boorsma, K., Chasapogianis, P., Manolas, D., Stettner, M., & Reijerkerk, M. *Comparison of models with respect to fatigue
load analysis of the INNWIND.EU and the AVATAR RWT.* Deliverable D4.6 of the EU project AVATAR,
September 2016.

Boorsma, K., Grasso, F., & Holierhoek, J. *Enhanced approach for simulation of rotor aerodynamic loads.* Energy Research
475   Center of the Netherlands, ECN-M-12-003, 2012.

Boorsma, K., Wenz, F., Aman, M., Lindenburg, C., & Kloosterman, M. *TKI WOZ VortexLoads final report.* TNO 2019
R11388, September 2019.

Duncan, J. *Observational Analyses of the North Sea low-level jet* . TNO R11428, November 2018 .

Gilbert, C., Messner, J. W., Pinson, P., Trombe, P. J., Verzijlbergh, R., van Dorp, P., & Jonker, H. (2020). Statistical post-
480   processing of turbulence-resolving weather forecasts for offshore wind power forecasting. Wind Energy, 23(4),
884–897. https://doi.org/10.1002/we.2456

Hersbach, H., Bell, B., Berrisford, P., Hirahara, S., Horányi, A., Muñoz-Sabater, J., … Thépaut, J. N. (2020). The ERA5
global reanalysis. *Quarterly Journal of the Royal Meteorological Society*, 146(730), 1999–2049.
https://doi.org/10.1002/qj.3803

485   Jonkman, B. *TurbSim User Guide.* NREL/TP-500-46198, 2009.

Lindenburg, C. *PHATAS Program for Horizontal Axis Turbine Analysis and Simulation.* Energy Research Center of the
Netherlands, ECN, ECN-I-05-005, 2005.

Mann J. 1998. Wind field simulation. *Probab. Eng. Mech.* 13:269‒82

Mehta, D., van Zuijlen, A. H., Koren, B., Holierhoek, J. G., & Bijl, H. (2014). Large Eddy Simulation of wind farm
490   aerodynamics: A review. *Journal of Wind Engineering and Industrial Aerodynamics*, 133, 1–17.
https://doi.org/10.1016/j.jweia.2014.07.002

Storey, R. C., Norris, S. E., Stol, K. A., & Cater, J. E. (2013). Large eddy simulation of dynamically controlled wind turbines
in an offshore environment. *Wind Energy*, 16(6), 845–864. https://doi.org/10.1002/we.1525

Sathe, A., Gotschall, J., & Courtney, M. *Can Wind Lidars measure turbulence.* Journal of Atmospheric and Oceanic
495   Technology, Volume 28, July 2011.

Savenije, F., Gonzalez Salcedo, A., Martin San Roman, R., Lampropoulos, N., Barlas, A., Sieros, G., . . . Maeder, T. *Evaluation of the new design, The advanced Reference Wind Turbine.* Deliverable 1.7 of the EU project AVATAR, December 2017.

Schalkwijk, J., Jonker, H. J. J., Siebesma, A. P., & Bosveld, F. C. (2015). A Year-Long Large-Eddy Simulation of the
500   Weather over Cabauw: an Overview. *Monthly Weather Review*, 143, 828–844. https://doi.org/10.1175/MWR-D-14-00293.1

Schepers, J.G. *Final Report of the EU project AVATAR.* http://www.eera-avatar.eu/fileadmin/avatar/user/AVATAR_final_report_v26_2_2018.pdf, 2018 (Accessed December 17, 2019).

Schepers, J. G. *Engineering models in Wind Energy Aerodynamics.* TUDelft, PhD thesis, November 2012.

505 Sieros, G., Lekou, D., Chortis, D., Chaviaropoulos, P., Munduate, X., Irissarri, A., . . . Reijerkerk, M. *Design of the AVATAR RWT rotor.* Deliverable D1.2 of the EU project AVATAR, January 2015.

Stettner, M., Irissari Ruiz, A., Madsen, H., Verelst, D., Croce, A., Sartori, L., . . . Reijerkerk, M. *Evaluation and cross-comparison of te AVATAR and INNWIND.EU RWT's.* Deliverable D1.3 of EU project AVATAR April 2015

Veers, P., Dykes, K., Lantz, E., Barth, S., Bottasso, C. L., Carlson, O., … Wiser, R. (2019). Grand challenges in the science
510   of wind energy. *Science*, *366*(6464), eaau2027. https://doi.org/10.1126/science.aau2027

Werkhoven, E., & Verhoef, J. *Offshore Meteorological Mast IJmuiden.* Energy Research Center of the Netherlands, ECN-Wind-Memo 12-010, 2012.

Wiegant, E., & Verzijlbergh, R. (2019). GRASP model description & validation report. Retrieved from https://www.dutchoffshorewindatlas.nl/binaries/dowa/documents/reports/2019/12/05/whiffle-report---grasp-model-
515   description-and-validation-report/grasp_description_validation.pdf

520

525